*29th EPS Conference on Plasma Phys. and Contr. Fusion Montreux, 17-21 June 2002 ECA Vol. **26B**, P-2.065 (2002)*

# DIII–D Quiescent Double Barrier Regime Experiments and Modeling

T.A. Casper,[1] K.H. Burrell,[2] J.C. DeBoo,[2] E.J. Doyle,[3] P. Gohil,[2] C.M. Greenfield,[2] R.J. Groebner,[2] R.J. Jayakumar,[1] T.B. Kaiser,[1] J.E. Kinsey,[4] C.J. Lasnier,[1] L.L. Lao,[2] M.A. Makowski,[1] G.R. McKee,[5] R.A. Moyer,[6] L.D. Pearlstein,[1] T.L. Rhodes,[3] D.L. Rudakov,[6] G.M. Staebler,[2] and W.P. West[2]

[1]*Lawrence Livermore National Laboratory, P.O. Box 808, Livermore, California 94551 USA*
[2]*General Atomics, P.O. Box 85608, San Diego, California 92186-5608 USA*
[3]*University of California, Los Angeles, Box 951597, Los Angeles, California 20742 USA*
[4]*Lehigh University, Bethlehem, Pennsylvania 18015 USA*
[5]*University of Wisconsin, Madison, Wisconsin, 53706-1687 USA*
[6]*University of California, San Diego, 9500 Gilman Drive, La Jolla, California 92093 USA*

Discharges characteristic of the quiescent double barrier (QDB) regime [1] are attractive for development of advanced tokamak (AT) scenarios relevant to fusion reactors [2] and they offer near term advantages for exploring and developing control techniques. We continue to explore the QDB regime in DIII–D to improve understanding of formation and control of these discharges and to explore scaling to steady-state reactors. The formation of an internal transport barrier (ITB) provides a naturally peaked core pressure profile. This peaking in density in combination with the H–mode-like edge barrier and pedestal provide a path to high performance. We have achieved $\beta_N H_{89P} \sim 7$ for several energy confinement times ($\leq 25\ \tau_E$). We discuss here a combination of modeling and experiments using electron cyclotron heating (ECH) and current drive (ECCD) to demonstrate steady state, current-driven equilibria and control of the current distribution, safety factor $q$, and density profile.

Experimental conditions leading to formation of the QDB discharge require establishing two distinct and separated barrier regions, a core region near $\rho \sim 0.5$ and an edge barrier outside $\rho > 0.95$, $\rho$ is the square root of toroidal flux (radial coordinate). A region of higher transport due to a change in polarity of the E×B shearing rate [1] separates the core barrier from the H–mode edge. It is this separation in barriers that so far has required use of counter-NBI to establish QDB conditions. Balanced NBI should also allow this separation of barriers. The edge corresponds to the quiescent H–mode (QH) conditions [3]. In this quiescent edge region, the normally observed transient loss associated with edge-localized-mode (ELM) activity is replaced with a steady particle loss driven by a coherent oscillation residing outside the pedestal region. This edge harmonic oscillation (EHO) [2] typically exhibits 2 or 3 harmonics of a fundamental frequency near 10 kHz. We find this combination of a core ITB and the QH–mode edge to be extremely robust and to produce slowly varying, high performance discharge parameters, Fig. 1, for long durations ~ 3 s. These conditions are generally limited by the duration of the NBI system and a slow evolution to lower $q$ values as the Ohmic current moves inward on the resistive time scale for diffusion.

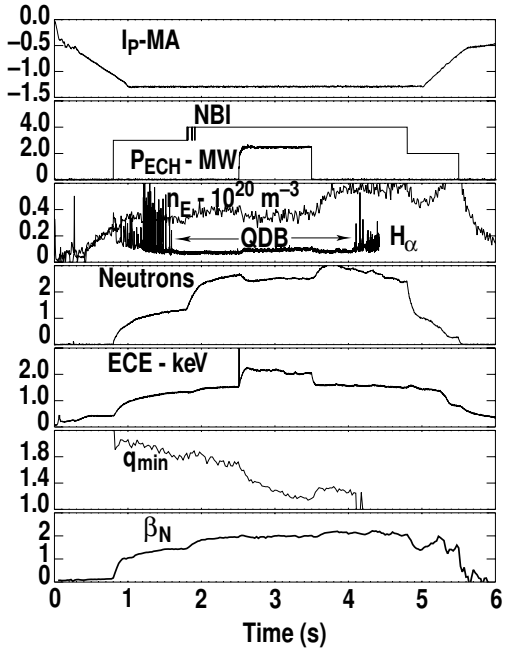


*Fig. 1. Discharge conditions for QDB shot with ECH.*

The ECH/ECCD system on DIII–D now comprises five megawatt-class gyrotrons capable of long pulse operation. Currently, 3 MW of power is available for pulse lengths up to 2 s. Future capability will provide up to 6 MW for a 10 s duration. Using Corsica [4] simulations, we explore the possibility of extending such QDB discharges to non-inductively current-driven steady-state

employing a combination of ECH and ECCD to drive current and control the $q$ profile. In these simulations, we use values for thermal diffusivities, $\chi_I$ and $\chi_E$, measured in an earlier non-EC-sustained QDB discharge (shot 103818) to evolve temperatures under conditions of ECH/ECCD. We assume no degradation in confinement due to this additional auxiliary power. The equilibrium is evolved using the Toray-GA [5] ray tracing code for EC heating and current drive and the NFREYA [6] code with orbits for NBI. We have not used particle transport in these simulations and, instead, fix the electron density (and $Z_{eff}$) at the measured values over the initial simulation interval and then hold the profile fixed in time outside the interval where measurements are available. The fast-ion particle density is determined from the NBI model and this, in turn, determines the thermal deuterium density. In Fig. 2, we show the evolution of the integrated current components to a QDB steady-state. We note that the bulk of the evolution occurs within the first 10 s and the remaining time evolution is required to achieve the non-inductively driven state with $J_{OH}=0$. In steady-state simulations, we constrain the loop voltage at $\rho=1$ to be zero from the on-set of EC injection at 1.9 s. to achieve the non-inductive current state. The initial OH current diffuses inwards and dissipates over time leading to the steady-state condition. The counter-NBI required to form a QDB has a negative impact on the final steady-state due to neutral beam current drive resulting from the unbalanced, tangential injection geometry. We require additional EC power to offset this NBCD, particularly on axis to control $q_0$. Since QDB formation relies on the sheared rotation profile, it may be achieved with balanced NBI. While balanced NBI is not currently possible on DIII–D, it is being seriously considered for a modification to the existing NBI installation.

Using the above simulation technique, we designed an experiment for the initial exploration of the effects of ECH/ECCD on a QDB plasma. This experiment addresses two issues, the early evolution towards steady-state and the ability of ECH/ECCD to control the current density and $q$ profiles on the modest time scales of the DIII–D experiment. While the global current diffusion times are long for these high temperature QDB discharges, as indicated in Fig. 2, a short pulse can determine the trajectory towards the steady-state. In these simulations, we force the loop voltage at $\rho=1$ to be zero to find steady-state conditions with no Ohmic current drive. We show in Fig. 2 the evolution of the total current predicted using 6.25 MW of EC power to reach a steady state at 40 s with $I_p$=–0.79 MA and an 80% bootstrap fraction. We also show the current drive components expected in DIII–D using 2.5 MW of EC power (plasma boundary), the power currently available for launch in the co-ECCD direction, defined here as along the total current and therefore opposite to the NBCD. Counter-NBI is achieved in DIII–D by reversing the direction of the inductively driven current as indicated by the negative plasma current, $I_p$, in the figures. In Fig. 3, we show the expected modification of the $q$-profile for antennas aimed for ECCD at $\rho$ = 0.35. We observe that the predicted evolution is well within the range of instrumentation and time-scales on DIII–D. Additional simulations indicated these effects are observable with ECH powers in excess of ~2 MW.

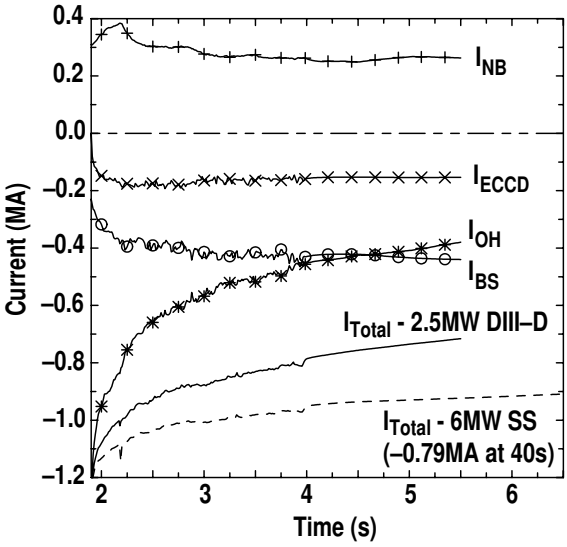


*Fig. 2. Design simulation to explore steady-state operation. Solid curves for DIII–D condition at 2.5 MW. Dashed curve is 6 MW steady-state simulation to 40 s.*

We recently conducted an experiment to demonstrate this effect of ECH/ECCD at controlling the $q$-profile in DIII–D, Fig. 1. Detailed analysis and modeling are just beginning. We injected a total of up to 2.3 MW of EC power using the four gyrotrons available for the

co-current drive launch. The EC power was typically initiated at 2.5 s, about 0.5 s after entering the QDB phase of the shot, to insure the QDB was well established. We find that the EHO existence and characteristics, and therefore the quality of the QDB discharge, were minimally affected by the high power EC injected. Hovever, the core profiles were modified by the additional heating and current drive. We observed clear evidence for modification of the *q* profile as is indicated in Fig. 1 by the reduction in $q_{min}$ during ECCD from 2.5 to 3.5 s. In Fig. 4 we observe the *q*-profile to be strongly modified in the location where ECCD is applied. Control of the current density, and therefore the *q* profile, using the EC system results from a combination of direct ECCD plus enhancement of the bootstrap current due to electron heating. These non-inductive current drive sources (including neutral beam current drive) are not individually distinguishable by the DIII–D diagnostic capabilities. We resort to distinguishing these components with our models for current drive; NBCD from the NFREYA code with orbits, Toray-GA for ECCD, and the NCLASS model for neoclassical bootstrap current drive. The *q*-profile modification begins after ~100 ms of ECCD as is determined by the local current relaxation time. This evolution of the minimum of *q* is consistent with our prior design simulations. For the results shown in Fig. 4, we used the time-dependently measured profiles of density, temperature and $Z_{eff}$ as input to the Ohm's law solver to determine the evolution of the equilibrium, current and *q*, subject to current drive components calculated. Multiple EC sources were simulated with the Toray-GA ray tracing code using angle settings and power from the experiment. We are currently extending this modeling with improved profile analysis and transport modeling to better estimate the combined effects of the various current drive components. The total driven current observed, ~60 kA, was slightly more than half of that originally predicted. The ray tracing code indicates that the location of the ECCD in this experiment was peaked at ρ~0.45 rather than the ρ~0.35 used for predictions. ECCD is quite sensitive to radial location and, in this region, current drive efficiency drops rapidly at larger radii. This could explain the lower total driven current for these shots. During our experimental run, there was insufficient time to scan the antenna aiming and optimize the effects due to ECCD.

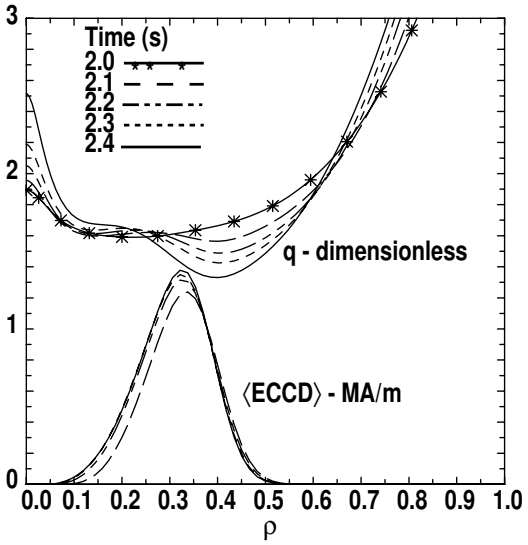


*Fig. 3. q profile evolution at start of ECH for experiment design: 2.5 MW ECH at ρ=0.35 with fixed χ, $n_e$, and $Z_{eff}$*

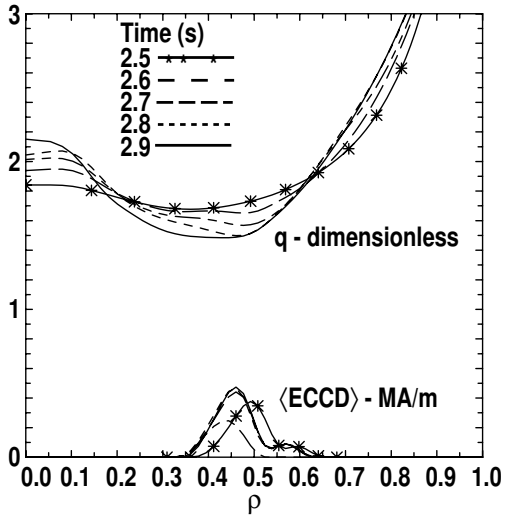


*Fig. 4. Ohm's law analysis of 110854, 2.2 MW of ECH at ρ=0.45, using measured density and temperature profiles.*

In addition to control of the q profile, we observed the injection of EC power to modify the density profile near the axis and reduce the density peaking; this effect was not included in the experiment design simulations. As shown in Fig. 5, the on-axis electron density (Thomson scattering) drops significantly during the ECH phase but the profile at large ρ remains essentially unaffected. This indicates our ability to control the density peaking and,

therefore, possibly the beta limits achievable. In most of our QDB shots we also observe the accumulation of high Z impurities, mostly copper and nickel, whose source is as yet unknown. During the EC injection, we observed a considerable reduction of this high-Z impurity concentration indicating the capability for EC control of the impurity content as well. Our initial estimates indicate that the impurity reduction exceeds the reduction in the on-axis electron density. Detailed analysis and modeling are underway to explore these effects.

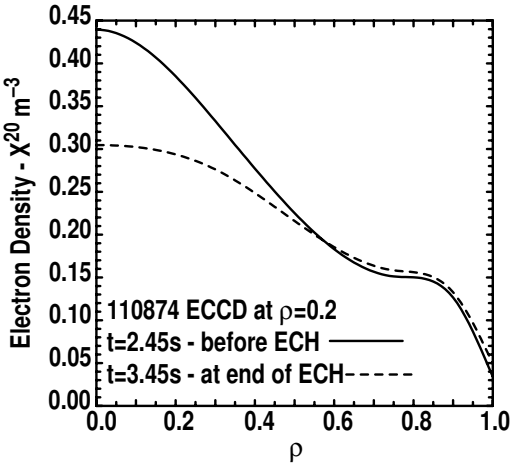


*Fig. 5. Density peaking control with ECH 110874, 2.3 MW ECH at ρ~0.2*

In summary, our simulations demonstrate the potential for scaling the QDB discharge conditions to steady-state and we predict the existence of a fully non-inductively driven state with relatively high bootstrap current fraction, ~80%. The main detriment is the reliance on counter-NBI to access the QBD regime and this requires use of high power ECCD to maintain the steady state. QDB discharge conditions provide a robust, high-performance plasma suitable for developing control capabilities needed for AT plasmas. Based on these simulations, we designed an experiment to test current profile control using the ECCD system on DIII–D. In the ensuing experiment, we injected in excess of 2 MW of EC power to successfully demonstrate the capability for control of the $q$ profile in a stable manner. We also established the possibility for control of the density peaking factor and the high-Z impurities. Modification of density peaking does not depend strongly on the antenna aiming whereas control of $q_{\min}$ is highly dependent on aiming to adjust the current drive radial location. We only recently conducted these experiments and analysis is currently under way to determine the contributions due to direct ECCD and bootstrap current drive and to develop the current and density control capabilities.

## ACKNOWLEDGMENT

Work supported by U.S. Department of Energy under Contracts W-7405-ENG-48, DE-AC03-99ER54463, and Grants DE-FG03-01ER54615, DE-FG02-92ER54141, DE-FG03-96ER54373, and DE-FG03-95ER54294.

## REFERENCES

[1] C.M. Greenfield, et al., Phys. Rev. Lett. **86**,4544 (2001).
[2] E.J. Doyle, et al., Plasma Phys. Control. Fusion **43**, A95 (2001).
[3] K.H. Burrell, et al., 2001 Phys. Plasmas **8** 2153.
[4] T.A. Casper, *et al*., 27th EPS Conference on Controlled Fusion and Plasma Physics, 12-16 June 2000, Budapest, Hungary.
[5] Y.R. Lin-Liu, et al., Radio Frequency Power in Plasmas: 12th Topical Conference, CP403 (195) 1997.
[6] R.J. Goldston, et al., J. Comp. Physics **43**, 61 (1981).